Daisuke Miyazaki, Katsushi Ikeuchi,
"Polarization-based Shape Estimation of Transparent Objects for Digitizing Cultural Assets,"
in Proceedings of International Symposium on the CREST Digital Archiving Project,
pp.34-41, Tokyo, Japan, 2005.03

http://www.cvl.iis.u-tokyo.ac.jp/~miyazaki/

Polarization-based Shape Estimation of Transparent Objects for Digitizing Cultural Assets

Daisuke Miyazaki Katsushi Ikeuchi

Department of Computer Science
Graduate School of Information Science and Technology
The University of Tokyo
Japan
http://www.cvl.iis.u-tokyo.ac.jp/

Abstract

Though there are many cultural assets which are made of glasses, most of the existing methods cannot estimate the shape of transparent objects with enough accuracy. We propose a novel method for estimating the surface shape of transparent objects by analyzing the polarization state of the light. Existing methods slightly consider the reflection, refraction, and transmission of the light occurring inside a transparent object. We employ a polarization ray-tracing method to compute both the path of the light and its polarization state. Our proposed iterative computation method estimates the surface shape of the transparent object by minimizing the difference between the polarization data rendered by the polarization ray-tracing method and the polarization data obtained from a real object.

1. Introduction

Digitizing the 3D geometrical data of cultural assets made of glasses is considered to be highly important because there is a possibility that those cultural assets might be damgaed or lost. Therefore, a technique for estimating the shape of transparent objects is strongly required in order to hand down such important cultural assets to our posterity. However, few methods have been proposed for estimating the shape of transparent objects, because of the difficulty of treating with the internal reflection or the inter-reflection, which are the phenomena that the light not only reflects at the surface of the transparent object but also transmits into the object and causes multiple reflection and transmission inside it. This paper presents a novel method for estimating the surface shape of transparent objects by analyzing the polarization of transparent objects.

Polarization is a phenomenon in which the light oscillates in one direction. Recently, research to estimate the object shape by using polarization has increased. Koshikawa and Shirai [1] estimated the surface normal of specular polyhedrons by analyzing circular polarization. They used a method called Mueller Calculus to calculate the polarization state of the light. Wolff and Boult [2] estimated the surface normal of a planer glass from two views. Rahmann and Canterakis [3] estimated the shape of specular objects from two or more views. Miyazaki et al. [4] estimated the shape and reflectance of specular objects and the illuminant direction from one view. Saito et al. [5] and Miyazaki et al. [6, 7] estimated the surface shape of transparent objects by means of polarization analysis. Unfortunately, because these methods do not consider internal reflections, they do not provide sufficient accuracy for estimating the shape of transparent objects. Other methods which estimate the 3D shape of transparent objects without using polarization have been proposed. Murase [8] estimated the shape of water surface by analyzing the undulation of the water surface. Hata et al. [9] estimated the surface shape of transparent objects by analyzing the deformation of the light projected onto the transparent objects. Ohara et al. [10] estimated the depth of the edge of transparent object by using shape-from-focus. Ben-Ezra and Nayar [11] estimated the parameterized surface shape of transparent objects by using structure-from-motion. These methods, however, do not estimate arbitrary shapes of transparent objects.

There are other works which treat with transparent objects such as environment matting [12–17] and reflection separation [18–21]; however, they do not provide rich information about the shapes of the transparent objects.

We simulate the internal reflection of transparent objects by using a method called polarization ray-tracing, and estimate the surface shape of transparent objects which have an arbitrary shape. In this paper, a forward-facing surface of the transparent object is called a frontal surface and an object surface facing away from the camera is called a rear surface. Our proposed method estimates the shape of the frontal surface by using polarization ray-tracing when the refractive index and the rear surface are given.

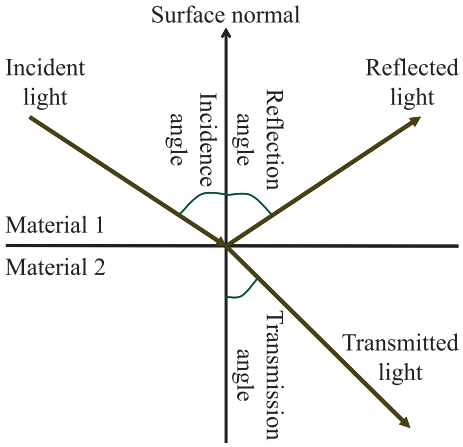

Figure 1: Reflection, refraction, and transmission.

The rest of the paper is organized as follows. In Section 2, we introduce the notations used in this paper; in Section 3, we describe the polarization ray-tracing method; and in Section 4, we explain our estimation method which solves the inverse problem of polarization raytracing method. Our measurement results are shown in Section 5, and our conclusions are presented in Section 6.

2. Terms and Notations

In this section, we will define the notations used in this paper. Theoretical detail of the principle of polarization, which appears in this section, is given in the literature [22].

Figure 1 describes the light reflected and transmitted between Material 1 and Material 2. Materials 1 and 2 may be, respectively, the air and the transparent object, and vice versa. Incidence angle, reflection angle, and transmission angle are defined in Figure 1. We assume that the surface of transparent objects is optically smooth; thus, the incidence angle is equal to the reflection angle. The transmission angle depends upon the incidence angle and the refractive index of the transparent object. The plane of incidence (POI) is a plane which includes the surface normal direction, the incident light direction, the reflected light direction, and the transmitted light direction.

The intensity ratio of reflected light to incident light is called intensity reflectivity R, and the intensity ratio of transmitted light to incident light is called intensity transmissivity T. Subscript $\parallel$ and $\perp$ represent the component parallel and perpendicular to POI, respectively. Thus, parallel and perpendicular components of intensity reflectivity are represented as $R_{\parallel}$ and $R_{\perp}$, respectively, while those of intensity transmissivity are represented as $T_{\parallel}$ and $T_{\perp}$, respectively. These values depend upon the incidence angle and the refractive index.

The polarization state of the light is calculated by observing the object with the monochrome camera, which has a linear polarizer in the front. For a certain pixel, we denote

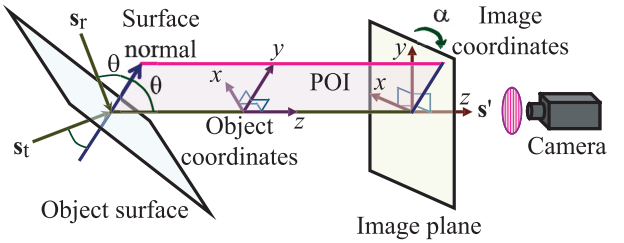

Figure 2: Reflected and transmitted light observed by the camera.

the maximum intensity observed by rotating the polarizer as $I_{\max}$ and the minimum as $I_{\min}$. The angle of the polarizer when the maximum intensity $I_{\max}$ is observed is called the phase angle ψ. This angle is defined as the angle from $+y$ axis to $-x$ axis in camera coordinates.

Suppose the geometrical setup when the reflected light is observed from the camera (Figure 2). The cross section of the POI and image plane of the camera will be a straight line. The angle between this straight line and the $+y$-axis is called the POI angle α. This angle is also defined as the angle from $+y$-axis to $-x$-axis in camera coordinates.

3. Polarization Ray-tracing

3.1. Mueller Calculus

A conventional ray-tracing method renders a 2D image from 3D geometrical shape data of transparent objects or other kind of objects. In this paper, we call the ray-tracing method which considers the polarization effect the polarization ray-tracing method.

The algorithm of the polarization ray-tracing method can be divided into two parts. For the first part, the calculation of the propagation of the ray, we employ the same algorithm used in the conventional ray-tracing method. For the second part, the calculation of the polarization state of the light, there are three famous methods: Mueller Calculus, Jones Calculus [23], and the method which uses the coherence matrix [22]. In this paper, we employ Mueller Calculus, because of its simplicity of description, along with its ease of understanding and implementation. These three methods have almost identical functions; thus, all discussions presented in this paper are also applicable to other calculi. We will present a brief overview of Mueller Calculus in the following pages; however, we will leave the details to the literature [23].

In Mueller Calculus, the polarization state of the light is represented as Stokes Vector $\mathbf{s} = (s_0, s_1, s_2, s_3)^T$. The Stokes Vector is a 4D vector. Its first component s_0 represents the intensity of the light; its second component s_1 represents the horizontal power of the linear polarization; its third component s_2 represents the $+45°$-oblique power of the linear polarization; and its fourth component s_3 represents the power of the right circular polarization. The

Mueller Matrix $\mathbf{M}$, which is 4×4 matrix, represents how the object changes the polarization state of the light. The operation of Mueller Calculus is a linear operation.

3.2. Mueller Matrix

First, we introduce a method for calculating the polarization state of the reflected light and the transmitted light when the POI angle is $0°$; after that, we introduce a method for the case when the POI angle is not $0°$.

Mueller Matrices of reflection $\mathbf{R}$ and transmission $\mathbf{T}$ when the POI angle is $0°$ are represented as follows:

$$\mathbf{R} = \begin{pmatrix} (R_\perp + R_\parallel)/2 & (R_\perp - R_\parallel)/2 & 0 & 0 \\ (R_\perp - R_\parallel)/2 & (R_\perp + R_\parallel)/2 & 0 & 0 \\ 0 & 0 & \sqrt{R_\perp R_\parallel} & 0 \\ 0 & 0 & 0 & \sqrt{R_\perp R_\parallel} \end{pmatrix} \quad (1)$$

$$\mathbf{T} = \begin{pmatrix} (T_\perp + T_\parallel)/2 & (T_\perp - T_\parallel)/2 & 0 & 0 \\ (T_\perp - T_\parallel)/2 & (T_\perp + T_\parallel)/2 & 0 & 0 \\ 0 & 0 & \sqrt{T_\perp T_\parallel} & 0 \\ 0 & 0 & 0 & \sqrt{T_\perp T_\parallel} \end{pmatrix} . \quad (2)$$

Thus, if we have a light ray with the Stokes Vector $\mathbf{s}$ impinged on an object, then the Stokes Vector of reflected light will be $\mathbf{Rs}$, when the POI angle is $0°$. The same thing can also be said of the transmitted light.

Figure 2 illustrates the case when the POI angle is α. Figure 3 explains how to calculate the reflected light for this case. The reflection matrix $\mathbf{R}$ is always multiplied to the Stokes Vector whose POI angle is transformed to $0°$. So, we first rotate the incident Stokes Vector $\mathbf{s}$ with the angle $-\alpha$. After that, $\mathbf{R}$ is multiplied to the transformed Stokes Vector. Finally, the Stokes Vector is rotated again with the angle α in order to restore the original coordinates. The resulting Stokes Vector $\mathbf{s}'$ is as follows:

$$\mathbf{s}' = \mathbf{C}(\alpha)\mathbf{R}\mathbf{C}(-\alpha)\mathbf{s} \quad , \quad (3)$$

where rotation matrix $\mathbf{C}$ is given as:

$$\mathbf{C}(\alpha) = \begin{pmatrix} 1 & 0 & 0 & 0 \\ 0 & \cos 2\alpha & -\sin 2\alpha & 0 \\ 0 & \sin 2\alpha & \cos 2\alpha & 0 \\ 0 & 0 & 0 & 1 \end{pmatrix} . \quad (4)$$

As for the case in Figure 2, observed light is a composition of reflected light and transmitted light. Thus, the Stokes Vector $\mathbf{s}'$ of the observed light is calculated as follows:

$$\mathbf{s}' = \mathbf{C}(\alpha)\mathbf{R}\mathbf{C}(-\alpha)\mathbf{s}_r + \mathbf{C}(\alpha)\mathbf{T}\mathbf{C}(-\alpha)\mathbf{s}_t \quad , \quad (5)$$

where Stokes Vectors of the incident light are represented as $\mathbf{s}_r$ and $\mathbf{s}_t$, and where $\mathbf{s}_r$ and $\mathbf{s}_t$ represent the lights which are set in the origin of the reflection and transmission, respectively.

3.3. Phase Shift

If an incidence angle is larger than the critical angle, then the light does not transmit and totally reflects. This phenomenon is called total reflection and occurs when the light is inside the object. Critical angle is calculated from the relative refractive index. Phase of the reflected light shifts when the total reflection occurs. Thus, for the total reflection, the following matrix $\mathbf{D}$ is used instead of the reflection Mueller Matrix $\mathbf{R}$:

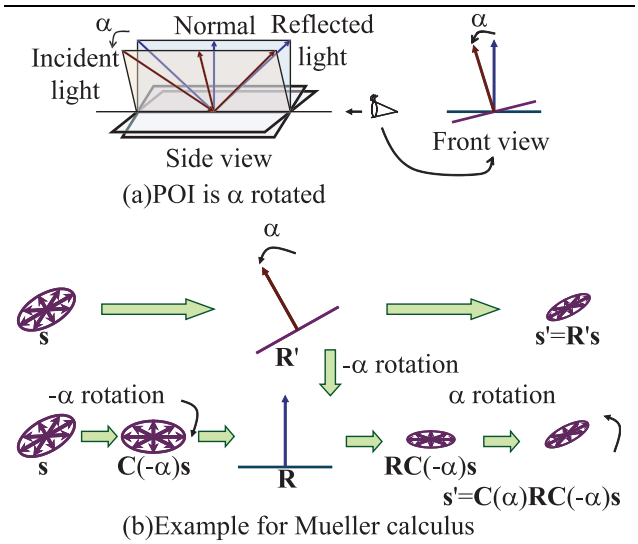

Figure 3: Calculation example of rotation Mueller Matrix for reflection.

$$\mathbf{D}(\delta) = \begin{pmatrix} 1 & 0 & 0 & 0 \\ 0 & 1 & 0 & 0 \\ 0 & 0 & \cos\delta & \sin\delta \\ 0 & 0 & -\sin\delta & \cos\delta \end{pmatrix} , \quad (6)$$

where δ is the amount of the phase shift, calculated by using the formula given in the literature. δ depends upon the incidence angle and the relative refractive index.

When the incidence angle is less than the Brewster Angle, the phase of the reflected light will be inverted; thus, the matrix $\mathbf{D}(180°)$ should be multiplied from the left to the reflection Mueller Matrix. The Brewster Angle depends upon the relative refractive index.

3.4. Degree of Polarization

Because the linear polarizer is used in this research, the fourth parameter s_3 of the Stokes Vector cannot be determined. The relationship between the Stokes Vector $(s_0, s_1, s_2)^T$ and $I_{\max}$, $I_{\min}$, ψ is:

$$\begin{pmatrix} s_0 \\ s_1 \\ s_2 \end{pmatrix} = \begin{pmatrix} 1 & 0 & 0 \\ 0 & \cos 2\psi & -\sin 2\psi \\ 0 & \sin 2\psi & \cos 2\psi \end{pmatrix} \begin{pmatrix} I_{\max} + I_{\min} \\ I_{\max} - I_{\min} \\ 0 \end{pmatrix} , \quad (7)$$

where $I_{\max}$, $I_{\min}$, and ψ are defined in Section 2. The degree of polarization (DOP) represents how much the light is polarized and is defined as follows:

$$\hat{\rho} = \frac{\sqrt{s_1^2 + s_2^2 + s_3^2}}{s_0} \quad . \quad (8)$$

However, linear polarizer can only calculate the following degenerated DOP:

$$\rho = \frac{I_{\max} - I_{\min}}{I_{\max} + I_{\min}} = \frac{\sqrt{s_1^2 + s_2^2}}{s_0} \quad . \quad (9)$$

For the remainder of this paper, we refer to the ratio calculated by Equation (9) as DOP.

3.5. Illumination Distribution

In this paper, we assume that all light sources are unpolarized, that the frontal surface of the object is uniformly illuminated from every direction with the same intensity, and that the light does not penetrate the object from the rear surface of the object.

4. Inverse Polarization Ray-tracing

In this section, we introduce our method for estimating the frontal surface shape of a transparent object using the DOP and the phase angle as inputs under the assumption that the refractive index and the backward-facing surface shape are given. Details of numerical algorithms are shown in the literature [24].

We denote the input polarization data as I_E. Polarization data are represented as an image(2-dimensionally distributed data) where the DOP and phase angle are set for each pixel. The polarizaiton ray-tracing explained in Section 3 can render the polarization data from the shape of transparent object. We denote such rendered polarization images as I_R. The shape of transparent objects is represented as the height H, set for each pixel. Heights partially differentiated by x and y are called gradient, and are represented as p and q, respectively:

$$p = H_x = \frac{\partial H}{\partial x}, \quad q = H_y = \frac{\partial H}{\partial y} \quad . \tag{10}$$

Surface normal $\mathbf{n} = (-p, -q, 1)^T$ is represented by these gradients.

The rendered polarization image I_R depends upon height and surface normal, so it can be represented as $I_R(H, p, q)$. Our problem is finding the best values to reconstruct a surface H that satisfies the following equation:

$$I_E = I_R(H, p, q) \quad . \tag{11}$$

We call this equation the "polarization ray-tracing equation" from the analogy of "image irradiance equation" used in the shape-from-shading problem.

A straightforward definition of the cost function which we want to minimize can be as follows:

$$\iint E_1(x, y)\, dxdy \quad , \tag{12}$$

where,

$$E_1 = (I_E - I_R(H, p, q))^2 \quad . \tag{13}$$

We will sometimes omit the variables (x, y) in the subsequent discussions for the simplicity of descriptions. I_R depends upon p, q, and H, while p, q, and H depend upon each other with Equation (10). Thus, cost function must be modified as follows:

$$\iint (\lambda E_1 + E_2)\, dxdy \quad , \tag{14}$$

where,

$$E_2 = (H_x - p)^2 + (H_y - q)^2 \quad . \tag{15}$$

λ is Lagrange's undetermined multiplier.

Euler equations which minimize Equation (14) are derived as follows:

$$p = H_x - \frac{\lambda}{2}\frac{\partial E_1}{\partial p} \tag{16}$$

$$q = H_y - \frac{\lambda}{2}\frac{\partial E_1}{\partial q} \tag{17}$$

$$H = \bar{H} - \frac{1}{4}(p_x + q_y) - \frac{\lambda}{8}\frac{\partial E_1}{\partial H} \quad , \tag{18}$$

where $\bar{H}$ is a 4-neighbor average of H.

Each of the above equations can be decomposed into two steps:

$$p \leftarrow H_x \tag{19}$$

$$p \leftarrow p - \lambda_1 \nabla E_1 \tag{20}$$

$$q \leftarrow H_y \tag{21}$$

$$q \leftarrow q - \lambda_2 \nabla E_1 \tag{22}$$

$$H \leftarrow \bar{H} - \frac{1}{4}(p_x + q_y) \tag{23}$$

$$H \leftarrow H - \lambda_3 \nabla E_1 \quad . \tag{24}$$

Here, λ_1, λ_2, and λ_3 are scalar values which are determined for each pixel and for each iteration step. ∇ in Equations (20)(22)(24) are,

$$\frac{\partial}{\partial p}, \quad \frac{\partial}{\partial q}, \quad \frac{\partial}{\partial H}, \tag{25}$$

respectively. As for Equations (19)(21)(23), A_x can be discretized, for example, as follows:

$$A_x(x, y) = \frac{1}{2}(A(x+1, y) - A(x-1, y)) \quad . \tag{26}$$

First, we set initial values of the shape H for each point of frontal surface. Next, p and q are calculated by Equations (19)(21). Then, we solve Equations (20)(22). λ_1 and λ_2 should be optimal values; thus, we use Brent's method to determine λ_1 and λ_2 which minimize the error function E_1. After computing p and q at every pixel, we solve Equation (23) by the relaxation method to determine the height H. Ikeuchi solved the relaxation problem by using the Jacobi method [25], while Horn [26] solved it by means of the successive over-relaxation method. We use the alternating-direction implicit method to increase the speed of computation.

Also, we do not choose to solve Equation (24) by Brent's method because the error function E_1 depends upon the change of surface normal rather than on the change of height. Another reason is that the error function E_1 smoothly changes when the surface normal changes, but it does not smoothly change when the height changes. This fact was empirically proved in the preliminary experiments.

To conclude, the frontal surface shape of transparent object is estimated by an iterative computation, where each

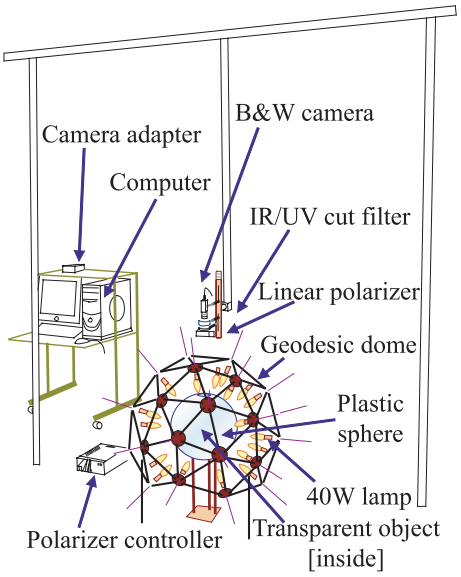

Figure 4: Acquisition System "Cocoon".

step of iteration solves Equations (19)–(23), and the iteration stops when Equation (12) is minimized. There are two reasons why we use Equations (19)–(23) instead of Equations (16)–(18): (1) If we solve Equations (16)–(18) simultaneously by setting an arbitrary value λ, a parameter tuning problem will occur where λ must be set to an optimal value in order to stably solve these equations; (2) We can apply adequate numerical algorithms for each of Equations (19)–(23).

5. Measurement Result

5.1. Acquisition System

For obtaining polarization data, we developed an acquisition system, which we named "Cocoon" (Figure 4). The target object is set inside the center of the plastic sphere whose diameter is 35cm. This plastic sphere is illuminated by 36 incandescent lamps. These 36 light sources are almost uniformly distributed spatially around the plastic sphere. The plastic sphere diffuses the light that comes from the light sources, and it behaves as a spherical light source, which illuminates the target object from every direction. The target object is observed by monochrome camera from the top of the plastic sphere, which has a hole on the top. Linear polarizer is set in front of the camera. We put the target object on the black pipe to avoid the incoming light from the rear surface. The camera, object, and light sources are fixed. From four images taken by rotating the polarizer at $0°$, $45°$, $90°$, and $135°$, we calculate $I_{\max}$, $I_{\min}$, and ψ (Section 2).

5.2. Rendering Results

Before estimating the shape of the transparent object, we analyzed the rendered image of forward polarization ray-tracing (Section 3).

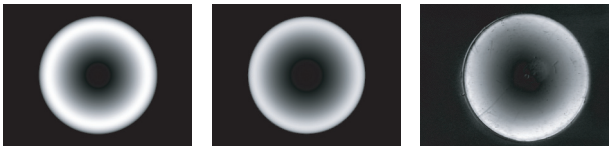

(a) (b) (c)

Figure 5: DOP image; (a) rendered by polarization raytracing, (b) obtained from real object, and (c) rendered by assuming that the internal reflection does not occur.

From the spherical part, we observed a transparent acrylic hemisphere, whose refractive index is 1.5 and diameter was 3cm. We assumed that the illumination was distributed uniformly from all directions with the same intensity and that the bottom surface of the object, a disk, was not illuminated.

Rendered polarization image of polarization ray-tracing is shown in Figure 5(b), and real polarization image is shown in Figure 5(c). Here, each figure represents the DOP, where DOP 0 and DOP 1 are represented as black and white, respectively.

For comparison, a rendered image with no internal reflection is shown in Figure 5(a). This DOP image is rendered by assuming that the light which reflected at the object surface once is just observed and that the transmission does not occur. Apparently, Figure 5(a) is far from Figure 5(b) and Figure 5(c). The root mean square (RMS) error between real data (Figure 5(c)) and DOP data of no internal reflection (Figure 5(a)) was 0.31, while the RMS error between real data and polarization ray-tracing data (Figure 5(b)) was 0.18.

5.3. Simulation Results

5.3.1. 2D Hexagon

First, we will show the result of estimating the 2D shape of a simulation-generated object for evaluating the accuracy of our algorithm. This virtual transparent object is a hexagonal shape whose refractive index is 1.5. The object is represented as a dotted line in Figure 6. We rendered the polarization data of the object observed from the upper position to the lower direction, and after that, we estimated the frontal surface shape of the hexagon by using the rendered polarization data as input data. Illumination was distributed uniformly from any direction with the same intensity. The light was not illuminated at the bottom of the shape but was illuminated on the frontal surface.

The estimation result is illustrated in Figure 6. The dotted line is the ground truth, and the solid line is the estimated shape. Figure 6(a) indicates the initial value, and (b) and (c) indicate the results after 3 and 30 loops of the proposed method. A hemisphere is used as the initial state of the shape. The shape converged to the ground truth at 30

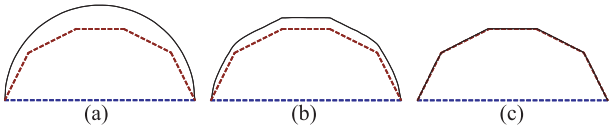

Figure 6: Simulation result of hexagon: (a)Initial state, (b)(c)result after 3, 30 loops, respectively.

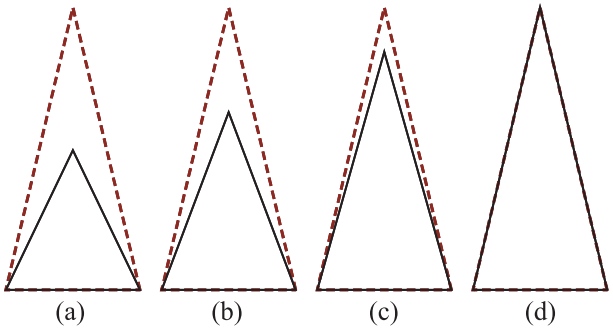

Figure 7: Simulation result of triangle: (a)Initial state, (b)–(d)result after 1–3 loops.

loops.

5.3.2. 2D Triangle

Another result is that of a 2D virtual transparent object, which is an isosceles triangle shape whose refractive index is 1.5 and whose two base angles are $76.6°$. Illumination is set to the same value as in Section 5.3.1. The object is observed from an apical angle. Frontal surface shape is estimated where the shape of the base is given.

The estimated result is illustrated in Figure 7. The dotted line is the ground truth, and the solid line is the estimated shape. Figure 7(a) is the initial state of the shape, and (b)–(d) is the resultant shape after 1–3 loops. Initial shape is set to be just the half height of the theoretical shape. The shape converged to the ground truth at 3 loops.

5.3.3. 3D Hemisphere

Next, we will present the simulation results in 3D. The target object is a virtual transparent hemisphere whose refractive index is 1.5. The estimation result is shown in Figure 8. Figure 8(a) represents the result of Miyazaki's method [6, 7] and, at the same time, it represents the intial value. Figure 8(b) is the result after 1 loop of our method. We calculated only 1 loop because the computation time is longer for the 3D case than for the 2D case. Figure 8(b) resembles the hemisphere more accurately than Figure 8(a) does.

5.4. Measurement Result of Real Object

Finally, we observed an acrylic transparent hemisphere from the spherical part, whose refractive index was 1.5 and diameter was 3cm. The frontal surface was a hemisphere and rear surface was a disk. The camera was set orthogonal to the disk. We assumed that the object was illuminated by

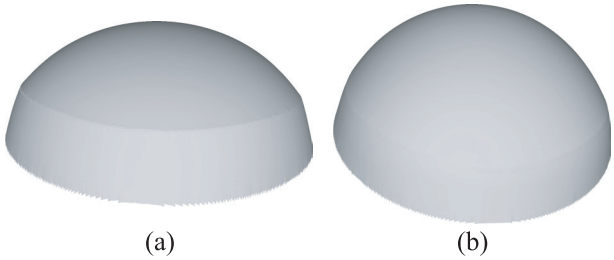

Figure 8: 3D simulation result: (a)Initial state (result of Miyazaki's method), (b)result after 1 loop.

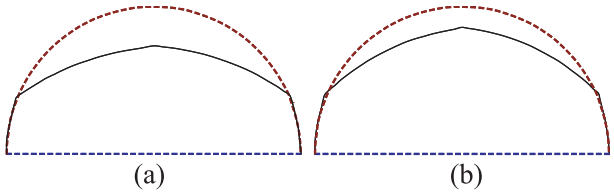

Figure 9: Estimation result: (a) Result of Miyazaki's method, (b) result after 5 loops with proposed method.

unpolarized light with uniform intensity from any direction. However, the disk, the rear surface, was not illuminated.

The evaluation was done in the 2D plane which was a cross section of the 3D object, which included the center of the base circle and the line perpendicular to that circle. A light ray which was inside this plane did not go out, and a light ray which was outside this plane did not come in. The proposed algorithm estimated the frontal surface shape, a semicircle, by using the polarization data of the 2D plane as input data.

The result of applying the proposed method is given in Figure 9(b). For comparison, the result of Miyazaki's method [6, 7] is shown in Figure 9(a). In Figure 9, the solid line represents the estimated shape, and the dotted line represents the ground truth. The shape computed by Miyazaki's method(Figure 9(a)) is used as an initial value for Figure 9(b). Figure 9(b) is the result after 5 loops. The shape did not deform any further even if we computed for more iteration.

The reason why the estimated result did not converge to the semicircle, which was the theoretical value, might be the lack of considering the illumination distribution. Although we had assumed that the object was illuminated uniformly with the same intensity from all directions, we now believe that this assumption might not strictly hold. Therefore, considering the illumination distribution will be our future work.

The RMS error between the estimated value and the ground truth was used to compare the accuracy between the proposed method and Miyazaki's method. The RMS error of the surface normal was $13.4°$ for Miyazaki's method and $8.99°$ for our method. The RMS error of the height was 3.22mm for Miyazaki's method and 1.95mm for our

method. Thus, we can conclude that our proposed method estimates the surface shape of transparent object more precisely than does Miyazaki's method.

6. Conclusion

In this paper, we have proposed a novel method for estimating the surface shape of transparent objects by minimizing the difference between the input polarization data taken by observing the transparent object and the computed polarization data rendered by the polarization ray-tracing method. At the end of this paper, we showed the measurement result of estimating the surface shape of a real transparent object by our proposed method, and the error of our method was about $2/3$ times smaller than those of previous methods [5–7].

It is impossible to analytically solve the inverse problem of polarization ray-tracing; thus, we estimated the transparent object shape by an iterative computation. We used a uniform illumination in this paper; however, Hata et al. [9] estimated the transparent object shape by an iterative computation where the object was illuminated by structured light. Ben-Ezra and Nayar [11] estimated the shape of a transparent object observed from many viewpoints by an iterative computation. Shape-from-silhouette(visual hull), which measures the object's shape from multiple views, has the defect that it cannot estimate a concave object; however, Nayar et al. [27], Wada et al. [28], and Yang et al. [29] estimated the concave shape of opaque object by iterative computation. To improve the precision of measuring the surface shape of transparent objects, we should probably observe the target object from multiple viewpoints or under various types of illumination. In any case, the iterative computation is considered to be necessary. Our paper provides the technique for measuring the surface shape of transparent objects using iterative computation, and this technique might be used as the basis for further developments.

Most of the artificial transparent objects have a planar base that enables them to stand by themselves. Also, the material (refractive index) of the artificial transparent objects is known in many cases. Thus, the assumption we adopted in this paper, "rear surface shape and refractive index are known," is effective in many cases. However, not all objects agree with such conditions; thus, we intend to develop a method which can measure the rear surface shape and refractive index at the same time as well as the frontal surface shape.

Acknowledgments

This research was supported in part by the Japan Science and Technology Agency under the Ikeuchi CREST project. Daisuke Miyazaki was supported by the Japan Society for the Promotion of Science. The authors thank the late Marie Elm for proofreading and editing this manuscript.

References

[1] K. Koshikawa and Y. Shirai, "A model-based recognition of glossy objects using their polarimetrical properties," *Advanced Robotics*, Vol. 2, No. 2, pp. 137-147, 1987.

[2] L. B. Wolff and T. E. Boult, "Constraining object features using a polarization reflectance model," *IEEE Trans. Patt. Anal. Mach. Intell.*, Vol. 13, No. 7, pp. 635-657, 1991.

[3] S. Rahmann and N. Canterakis, "Reconstruction of specular surfaces using polarization imaging," *Proc. IEEE Conf. Computer Vision and Pattern Recognition*, pp. 149-155, 2001.

[4] D. Miyazaki, R. T. Tan, K. Hara, and K. Ikeuchi, "Polarization-based inverse rendering from a single view," *Proc. IEEE Int'l Conf. Computer Vision*, pp. 982-987, 2003.

[5] M. Saito, Y. Sato, K. Ikeuchi, and H. Kashiwagi, "Measurement of surface orientations of transparent objects by use of polarization in highlight," *J. Opt. Soc. Am. A*, Vol. 16, No. 9, pp. 2286-2293, 1999.

[6] D. Miyazaki, M. Saito, Y. Sato, and K. Ikeuchi, "Determining surface orientations of transparent objects based on polarization degrees in visible and infrared wavelengths," *J. Opt. Soc. Am. A*, Vol. 19, No. 4, pp. 687-694, 2002.

[7] D. Miyazaki, M. Kagesawa, and K. Ikeuchi, "Transparent surface modeling from a pair of polarization images," *IEEE Trans. Patt. Anal. Mach. Intell.*, Vol. 26, No. 1, pp. 73-82, 2004.

[8] H. Murase, "Surface shape reconstruction of a nonrigid transparent object using refraction and motion," *IEEE Trans. Patt. Anal. Mach. Intell.*, Vol. 14, No. 10, pp. 1045-1052, 1992.

[9] S. Hata, Y. Saitoh, S. Kumamura, and K. Kaida, "Shape extraction of transparent object using genetic algorithm," *Proc. Int'l Conf. Pattern Recognition*, pp. 684-688, 1996.

[10] K. Ohara, M. Mizukawa, K. Ohba, and K. Taki, "3D modeling of micro transparent object with integrated vision," *Proc. IEEE Conf. Multisensor Fusion and Integration for Intelligent Systems*, pp. 107-112, 2003.

[11] M. Ben-Ezra and S. K. Nayar, "What does motion reveal about transparency?," *Proc. IEEE Int'l Conf. Computer Vision*, pp. 1025-1032, 2003.

[12] D. E. Zongker, D. M. Warner, B. Curless, and D. H. Salesin, "Environmental matting and compositing," *Proc. SIGGRAPH*, pp. 205-214, 1999.

[13] Y. Chuang, D. E. Zongker, J. Hindorff, B. Curless, D. H. Salesin, and R. Szeliski, "Environment matting extensions: towards higher accuracy and real-time capture," *Proc. SIGGRAPH*, pp. 121-130, 2000.

[14] Z. S. Hakura and J. M. Snyder, "Realistic reflections and refractions on graphics hardware with hybrid rendering and layered environment maps," *Proc. Eurographics Workshop on Rendering*, pp. 289-300, 2001.

[15] W. Matusik, H. Pfister, R. Ziegler, A. Ngan, and L. McMillan, "Acquisition and rendering of transparent and refractive objects," *Proc. Eurographics Workshop on Rendering*, pp. 267-278, 2002.

[16] Y. Wexler, A. W. Fitzgibbon, and A. Zisserman, "Image-based environment matting," *Proc. Eurographics Workshop on Rendering*, pp. 279-290, 2002.

[17] P. Peers and P. Dutré, "Wavelet environment matting," *Proc.*

Eurographics Workshop on Rendering, pp. 157-166, 2003.

[18] Y. Y. Schechner, J. Shamir, and N. Kiryati, "Polarization and statistical analysis of scenes containing a semireflector," *J. Opt. Soc. Am. A*, Vol. 17, No. 2, pp. 276-284, 2000.

[19] Y. Y. Schechner, N. Kiryati, and R. Basri, "Separation of transparent layers using focus," *Int'l J. Computer Vision*, Vol. 39, No. 1, pp. 25-39, 2000.

[20] R. Szeliski, S. Avidan, and P. Anandan, "Layer extraction from multiple images containing reflections and transparency," *Proc. IEEE Conf. Computer Vision and Pattern Recognition*, pp. 246-253, 2000.

[21] H. Farid and E. H. Adelson, "Separating reflections from images by use of independent component analysis," *J. Opt. Soc. Am. A*, Vol. 16, No. 9, pp. 2136-2145, 1999.

[22] M. Born and E. Wolf, *Principles of optics*, Pergamon Press, 1959.

[23] W. A. Shurcliff, *Polarized light: production and use*, Harvard University Press, 1962.

[24] W. H. Press, S. A. Teukolsky, W. T. Vetterling, and B. P. Flannery *Numerical recipes in C: the art of scientific computing*, Cambridge University Press, 1992.

[25] K. Ikeuchi, "Reconstructing a depth map from intensity maps," *Proc. Int'l Conf. Pattern Recognition*, pp. 736-738, 1984.

[26] B. K. P. Horn, "Height and Gradient from Shading," *Int'l J. Computer Vision*, Vol. 5, No. 1, pp. 37-75, 1990.

[27] S. K. Nayar, K. Ikeuchi, and T. Kanade, "Shape from interreflections," *Int'l J. Computer Vision*, Vol. 6, No. 3, pp. 173-195, 1991.

[28] T. Wada, H. Ukida, and T. Matsuyama, "Shape from shading with interreflections under a proximal light source: distortion-free copying of an unfolded book," *Int'l J. Computer Vision*, Vol. 24, No. 2, pp. 125-135, 1997.

[29] J. Yang, D. Zhang, N. Ohnishi, and N. Sugie, "Determining a polyhedral shape using interreflections," *Proc. IEEE Conf. Computer Vision and Pattern Recognition*, pp. 110-115, 1997.